Eur J Nucl Med Mol Imaging
DOI 10.1007/s00259-017-3643-2

ORIGINAL ARTICLE

Preclinical imaging characteristics and quantification of Platinum-195m SPECT

E. A. Aalbersberg[1] · B. J. de Wit – van der Veen[1] · O. Zwaagstra[2] · K. Codée – van der Schilden[2] · E. Vegt[1] · Wouter V. Vogel[1]

Received: 22 August 2016 / Accepted: 29 January 2017

Abstract
Aims In vivo biodistribution imaging of platinum-based compounds may allow better patient selection for treatment with chemo(radio)therapy. Radiolabeling with Platinum-195m (^{195m}Pt) allows SPECT imaging, without altering the chemical structure or biological activity of the compound. We have assessed the feasibility of ^{195m}Pt SPECT imaging in mice, with the aim to determine the image quality and accuracy of quantification for current preclinical imaging equipment.
Methods Enriched (>96%) ^{194}Pt was irradiated in the High Flux Reactor (HFR) in Petten, The Netherlands (NRG). A 0.05 M HCl ^{195m}Pt-solution with a specific activity of 33 MBq/mg was obtained. Image quality was assessed for the NanoSPECT/CT (Bioscan Inc., Washington DC, USA) and U-SPECT^{+}/CT (MILabs BV, Utrecht, the Netherlands) scanners. A radioactivity-filled rod phantom (rod diameter 0.85-1.7 mm) filled with 1 MBq ^{195m}Pt was scanned with different acquisition durations (10-120 min). Four healthy mice were injected intravenously with 3-4 MBq ^{195m}Pt. Mouse images were acquired with the NanoSPECT for 120 min at 0, 2, 4, or 24 h after injection. Organs were delineated to quantify ^{195m}Pt concentrations. Immediately after scanning, the mice were sacrificed, and the platinum concentration was determined in organs using a gamma counter and graphite furnace – atomic absorption spectroscopy (GF-AAS) as reference standards.
Results A 30-min acquisition of the phantom provided visually adequate image quality for both scanners. The smallest visible rods were 0.95 mm in diameter on the NanoSPECT and 0.85 mm in diameter on the U-SPECT^{+}. The image quality in mice was visually adequate. Uptake was seen in the kidneys with excretion to the bladder, and in the liver, blood, and intestine. No uptake was seen in the brain. The Spearman correlation between SPECT and gamma counter was 0.92, between SPECT and GF-AAS it was 0.84, and between GF-AAS and gamma counter it was0.97 (all $p < 0.0001$).
Conclusion Preclinical ^{195m}Pt SPECT is feasible with acceptable tracer doses and acquisition times, and provides good image quality and accurate signal quantification.

Keywords ^{195m}Pt · Small animal imaging · SPECT

Introduction

The anti-proliferative effects of platinum (Pt) complexes were observed in 1965 by Rosenberg et al. [1] and led to the introduction of cisplatin in clinical oncology in the 1970s. Forty years later cisplatin is still widely applied for the treatment of various cancers, most often combined with radiotherapy. Cisplatin-based concurrent chemoradiotherapy (CCRT) is considered a standard treatment option for stage II-III cancers of the lungs, head and neck, cervix, bladder, endometrium, and esophagus [2, 3]. In the last decade, other platinum compounds including carboplatin and oxaliplatin have also found a place in clinical practice, with similar benefits for selected indications [4].

Although cisplatin is widely used, it exhibits significant toxicity and resistance to treatment is a common problem. It has been estimated that only 8-11% of patients with head and neck cancer benefit from the addition of cisplatin to

✉ Wouter V. Vogel
w.vogel@nki.nl

[1] Department of Nuclear Medicine, The Netherlands Cancer Institute (NKI-AVL), Plesmanlaan 121, 1066 CX Amsterdam, The Netherlands

[2] Nuclear Research and Consultancy Group (NRG), Petten, The Netherlands

Published online: 11 February 2017

radiotherapy [5, 6], suggesting that a major percentage of patients are unnecessarily exposed to cisplatin toxicity [7]. Optimization of treatment requires a better understanding of the behavior of platinum-based chemotherapeutics in vivo, but tools to assess the biodistribution of these pharmaceuticals are currently lacking. Presently, platinum concentrations in tissues can only be determined in biopsy material, which are obtained invasively and do not represent the whole tumor [8]. A non-invasive method for determination of platinum concentrations would enable in vivo studies of pharmacokinetics, dosing, and factors affecting the distribution of platinum compounds and their relation to tumor response and toxicity.

The incorporation of a radioactive platinum isotope in platinum-based chemotherapies allows evaluation of tissue concentrations using various techniques, including non-invasive gamma camera imaging [9]. Radiolabeling can be achieved by substitution of the platinum atom with the radioactive isotopes ^{191}Pt, ^{193m}Pt, or ^{195m}Pt, each with their own physical characteristics [10, 11]. Based on its decay scheme with a favorable half-life and photon energy, ^{195m}Pt is considered the isotope most suitable for medical imaging.

Only a limited number of studies using radiolabeled cisplatin have been described in the literature. Some of these were limited to determining platinum concentrations in plasma or tissues using a well counter or autoradiography [12–14]. Scintigraphy has been attempted incidentally with various platinum isotopes, especially in the 1970s and 1980s [9, 11, 15–19] and in one more recent publication [20]. The available imaging studies show that tumors and normal tissues (liver, kidney, brain, and bowels) may vary significantly in accumulation of cisplatin, both in animals and in humans [18]. However, all published imaging studies employed planar scintigraphy, which suffers from superposition of the counts emitted from different internal structures and does not allow accurate quantification of uptake in tissues.

Over the last decades, gamma camera design has improved a great deal, especially in terms of sensitivity, spatial resolution and attenuation correction. The introduction of 3-dimensional (3-D) imaging using single photon emission computed tomography (SPECT) combined with computed tomography (CT) has enabled anatomical correlation and quantitative imaging [21]. These developments have also benefited pre-clinical imaging equipment, sparking new interest for in vivo biodistribution imaging.

The purpose of the current study was to investigate the feasibility and characteristics of ^{195m}Pt SPECT in mice using state-of-the-art preclinical SPECT/CT systems. We especially focused on the accuracy of in vivo concentration measurements compared to ex vivo measurements.

Materials and methods

Production of ^{195m}Pt

Platinum-195 m was produced by thermal neutron irradiation (n,γ) of enriched Platinum-194 contained in a quartz ampoule in the High Flux Reactor (HFR) in Petten, the Netherlands. After irradiation, a $H_2{}^{195m}PtCl_6$ solution of 52 MBq ^{195m}Pt/ml 0.05 M HCl was prepared with a specific activity of 33 MBq ^{195m}Pt/mg Pt at the end of irradiation (EOI). Part of the ^{195m}Pt solution was analyzed for radioactivity and radionuclide purity (^{197}Pt, ^{191}Pt ^{192}Ir, ^{194}Ir, ^{198}Au, ^{199}Au) using a high purity Germanium detector (HPGe) coupled to a multi-channel analyzer system. The energy window ranged from 50 to 1640 keV. Data were processed using NEMO software version 2.4.7 (NRG, van Dijken and Oudshoorn 2011).

Phantom study

Two preclinical SPECT/CT systems were evaluated for image characteristics using ^{195m}Pt: the NanoSPECT/CT (Bioscan Inc., Washington DC, USA) and the U-SPECT$^+$/CT (MILabs BV, Utrecht, the Netherlands). The resolution of ^{195m}Pt-SPECT was assessed using a radioactivity-filled rod phantom containing six sections with capillaries respectively 0.85, 0.95, 1.1, 1.3, 1.5, or 1.7 mm in diameter (Fig. 1). The distance between neighboring capillaries within each section equaled the diameter of the capillaries in that section. The phantom was filled with 1 MBq of ^{195m}Pt. Quantification of the NanoSPECT was determined with a dilution series of 1.5 ml Eppendorf tubes filled with 4, 2, 1, 0.5, 0.25, 0.125, 0.063, and 0.031 MBq of ^{195m}Pt in 1 ml.

Animal imaging study

The local animal ethics committee approved all animal studies. Mice were only scanned on the NanoSPECT, not on the U-SPECT$^+$ because this scanner was located in a different facility. Balb/c nude mice ($n = 4$), 13 weeks of age, received 133 MBq/kg $H_2{}^{195m}PtCl_6$ intravenously in the tail vein.

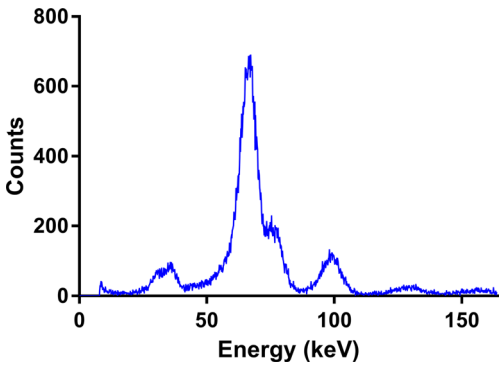

Fig. 1 Energy spectrum of $H_2{}^{195m}PtCl_6$ acquired on the NanoSPECT

SPECT/CT imaging of the four mice was performed under isoflurane anesthesia at 0, 2, 4, or 24 h after injection of ^{195m}Pt, respectively. Organs (kidneys, liver, blood pool over the heart, and brain) were delineated manually on fused SPECT/CT images to quantify organ uptake (counts/mm^3). Immediately after imaging, the mice were sacrificed and the major organs were collected, weighed, and processed for ex vivo platinum measurement.

SPECT imaging

For the NanoSPECT the four rotating NaI(TI) detectors (215 × 230 mm^2 each) were each shielded by a general-purpose pinhole mouse collimator with nine pinholes (pinhole diameter 1.4 mm, APT1). With this set-up the highest achievable reconstructed resolution is approximately 1.0 mm. The phantom study images were acquired in 24 angular stops with an angular increment of 3.75° in 25, 75, 150, and 300 s per projection, leading to 10, 30, 60, and 120 min of actual imaging time. The animal studies were acquired in 24 angular stops with an angular increment of 3.75° in 300 s per projection, leading to 120 min of actual imaging time. The two energy windows were set manually around the three major gamma peaks of ^{195m}Pt (65 keV and 67 keV peaks, range 59-75 keV and 99 keV peak, range 86-105 keV). Images were reconstructed using HiSPECT software (Scivis, Goettingen, Germany) with medium smoothing and resolution settings in 15 iterations, in isotropic voxels of 0.3 mm in three directions. No corrections were performed for attenuation, decay, or scatter as this was not possible in the software version provided with this imaging system. A CT scan was acquired for image correlation purposes. SPECT and CT images were fused using InVivoScope.

The U-SPECT+ system consists of three stationary NaI(TI) detectors (595 × 472 mm^2 each) that surround one cylindrical collimator, and, therefore, does not use angular steps to acquire images [22]. Images of the phantom were acquired for 120 min in list-mode with both the general-purpose mouse collimator (GP-M, 75 pinholes, pinhole diameter 0.6 mm) and the extra-ultra high sensitivity mouse collimator (XUHS-M, 54 pinholes, pinhole diameter 2.0 mm). The highest achievable reconstructed resolution is approximately 0.4 mm for the GP-M and 1.5 mm for the XUHS-M collimator. The energy windows were centered at 66 keV and 100 keV using a width of 15%. Image reconstruction was performed using the software provided by the manufacturer with an iterative reconstruction protocol, using the information from 10 min, 30 min, 60 min and 120 min counting, respectively, with a voxel size of 0.2 × 0.2 mm and slice thickness of 0.4 mm. Gaussian blur filters of 0.4, 0.8, and 1.2 mm full-width-half-maximum were applied to determine the optimum imaging quality. No corrections were performed for attenuation, decay, or scatter. No CT scan was acquired.

SPECT evaluation

All phantom SPECT images were evaluated visually for general image quality. The resolution was determined for both scanners by visual identification of the smallest separately visible rods. The sensitivity of the NanoSPECT scanner was determined from activity measurements with the Eppendorf tubes using a manually defined volume of interest (VOI), from which the count rate was related to the known activity concentration. The image quality of the animal SPECT images was assessed visually. The activity concentrations in different tissues / organs (kidneys, liver, blood pool and brain) were determined by manually drawing a VOI in these organs and recording the mean activity concentration. The accuracy and linearity of the measured activity concentrations on SPECT in vivo were determined by correlation with ex vivo measurement of different tissues, as described below.

Ex vivo platinum measurement

The ^{195m}Pt concentrations in collected tissues were measured using a well-type gamma counter (1480 Wizard, PerkinElmer) for 60 s with an energy window of 50 to 110 keV. In addition, total Pt concentrations (radioactive and non-radioactive combined) were measured using Graphite-furnace atomic absorption spectroscopy (GF-AAS). Tissue samples of approximately 100 mg were weighed and 1 ml of HNO_3 was added to the samples overnight. The samples were subsequently heated to 130 °C until 100 μl remained. Then, 0.5 ml of 1 M HCl was added, and the samples were reheated to 130 °C until 100 μl remained; this process was repeated once with 0.1 M HCl. The samples were diluted 10 fold in volume in measuring buffer containing 0.15 M NaCl and 0.2 M HCl and stored at -20 °C until analysis. Tissue analysis was performed using an atomic absorption spectrometer (SOLAAR MQZ Zeeman, Thermo Optek) with a GF95 graphite furnace and FS95/97 autosampler (Thermo Elemental). Reference samples with known platinum concentrations were used for calibration.

Data analysis

Statistical analyses were performed in GraphPad Prism version 6.0b for Mac OS X (GraphPad Software). The Spearman correlation test was used to evaluate relations between quantitative SPECT, GF-AAS, and gamma counter values.

Results

Production of ^{195m}Pt

Determination of the radionuclide purity in a sample of the analyzed solution showed 1.48E + 07 Bq ^{195m}Pt, 4.53E +

06 Bq of ^{197}Pt, 3.15E + 04 Bq of ^{191}Pt, 6.18E + 04 Bq of ^{192}Ir, 1.48E + 06 Bq of ^{194}Ir, 2.60E + 04 Bq of ^{198}Au, and 3.01E + 06 Bq of ^{199}Au at EOI, indicating that ^{195m}Pt comprised 62% of the total radioactivity at EOI. ^{197}Pt and ^{194}Ir have relatively short half-lives in comparison to that of ^{195m}Pt; that is 19.89 and 19.16h, respectively, versus 4.02 days. As a result, 77% of the total radioactivity was from ^{195m}Pt at 2 days after EOI, compared to 6% and 2% from ^{197}Pt and ^{194}Ir, respectively. ^{199}Au ($T_{1/2}$: 3.14 days) remained present for 14% of the total radioactivity at 2 days after EOI. Table 1 shows the radionuclide purity at each step during production and the experiment. Figure 1 shows an acquired spectrum on the NanoSPECT.

Phantom study

For the NanoSPECT, the resolution was visually determined at 0.95 mm (Fig. 2). The 0.95 mm rods were visible as separate rods at an acquisition time of 30 min. At 10 min duration the smallest visible rods were 1.1 mm. Extension of the scan time beyond 30 min did not improve the resolution further.

For the U-SPECT$^+$, the image quality was found to be optimal using the GP-M collimator and 0.8 mm FWHM Gaussian blurring. This resulted in good visibility of the 0.85 mm rods (the smallest rods present in the phantom, Fig. 3) at a scanning time of 30 min. Scanning longer than 30 min did not improve image quality significantly. However, with a coarser acquisition time of 10 min, use of the XUHS collimator (with larger pinholes and a lower specified spatial resolution) and 0.4 mm Gaussian blurring yielded better image quality compared to the GP collimator. With these settings, the 1.1 mm rods were separately visible.

Mouse imaging

Figure 4 shows SPECT images of four mice at different time points after intravenous injection of ^{195m}Pt. Imaging was performed for two h, as this was considered the maximum time to keep the animals under anesthesia. The general image quality was considered adequate, especially given the relative low dosage and intense accumulation in the tail. The kidneys and the bladder are clearly visualized, indicating high platinum uptake and excretion. Lower uptake, retention, and/or excretion are visible in the liver, blood pool and intestine. This strongly suggests a dominant renal clearance of $H_2{}^{195m}PtCl_6$. After 24 h the bladder was hardly visible anymore, whereas the kidney and liver uptake remained similar. This may indicate renal retention of platinum. The high activity concentrations in the tail of the mice are probably due to extravasation, probably due to the highly acidic platinum solution (pH 1-2). Figure 5 shows the distribution of ^{195m}Pt.

Quantification and ex vivo correlation

Quantification was based on the calibration curve determined with the dilution series of ^{195m}Pt and is shown in Fig. 6. The activity concentrations in the liver, kidneys, blood pool, and brain, as quantified on the SPECT images, correlated well with ex vivo measurements (Fig. 7). The correlation coefficient between SPECT and gamma counter was 0.92 ($p < 0.0001$), between GF-AAS and gamma counter 0.97 ($p < 0.0001$) and between SPECT and GF-AAS 0.84 ($p < 0.0001$).

Discussion

In this study we present the first preclinical SPECT images of ^{195m}Pt, showing its potential as a tracer to image the distribution of platinum-based compounds in vivo. The results indicate that quantitative ^{195m}Pt SPECT at sub-millimetric resolution is feasible in mice, and this characterizes the procedure for future applications. The isotope ^{195m}Pt can be incorporated into platinum-based compounds, thus enabling in vivo prediction of compound effectiveness and toxicity in individuals, and could be used for personalizing medicine with platinum-based chemotherapy.

To our knowledge, this is the first study to report high-resolution SPECT imaging of the isotope ^{195m}Pt in mice. Prior studies with clinical SPECT cameras have reported resolutions of approximately 12 mm at best. The gamma spectrum of ^{195m}Pt has three main photon peaks suitable for imaging, 65 keV, 67 keV, and 99 keV, which are of slightly lower energy than the photon peak of ^{99m}Tc (141 keV). Accordingly, imaging characteristics of ^{195m}Pt are theoretically expected to be somewhat sub-optimal compared to the mainstream

Table 1 Radionuclidic composition in percentage of the total activity at each step of the production and experiment.

	^{195m}Pt	^{197}Pt	^{191}Pt	^{192}Ir	^{194}Ir	^{198}Au	^{199}Au
$T_{1/2}$ (days)	4.02	0.83	2.86	73.8	0.80	2.7	3.14
End of Irradiation	61.82	18.92	0.13	0.26	6.18	0.11	12.57
Injection in mice	79.61	4.15	0.14	0.51	1.24	0.11	14.23
24 hours post-injection in mice	90.32	0.26	0.08	0.67	0.07	0.06	8.54
Phantom NanoSPECT	95.33	0.00	0.03	1.34	0.00	0.02	3.29
Phantom USPECT$^+$	98.51	0.00	0.00	0.77	0.00	0.00	0.71

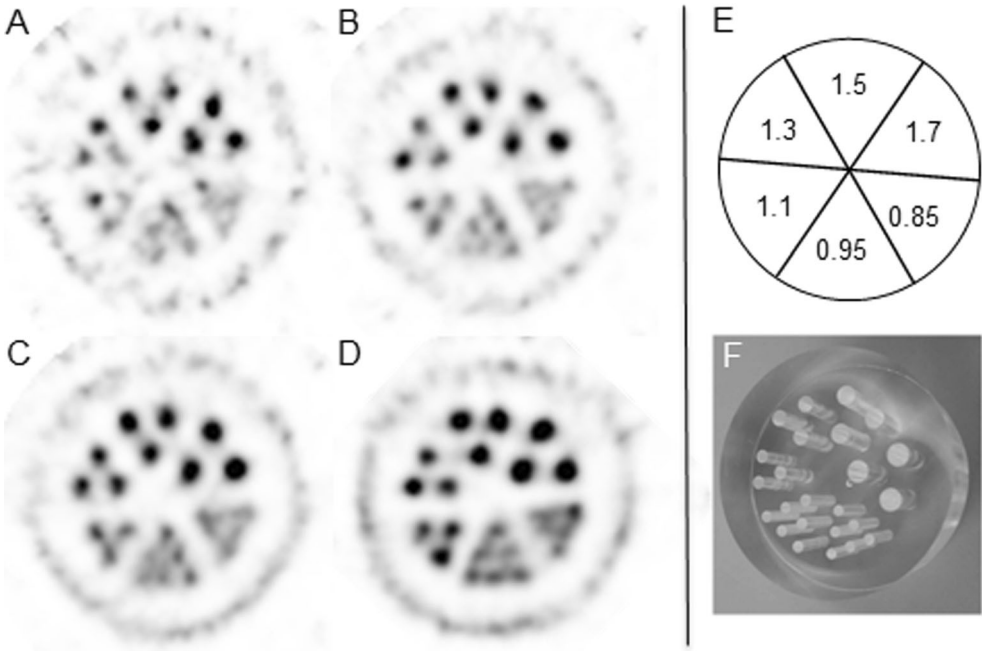

Fig. 2 Images of the radioactivity-filled rod phantom filled with 1 MBq of ^{195m}Pt acquired on the NanoSPECT in (**a**) 10 minutes, (**b**) 30 min, (**c**) 60 min, and (**d**) 120 min. (**e**) Diagram of the rod sizes in the phantom in millimeters. (**f**) A photograph of the radioactivity-filled rod phantom

isotope ^{99m}Tc, with higher photon scatter and attenuation especially in clinical imaging.

An important finding of this study is that ^{195m}Pt accumulation can be accurately quantified in mice using both SPECT systems. The data demonstrate a high correlation between the measured activity of ^{195m}Pt on SPECT and the tissue concentration of platinum measured ex vivo. Accurate quantification of ^{195m}Pt activity in vivo by SPECT is possible, with a linear

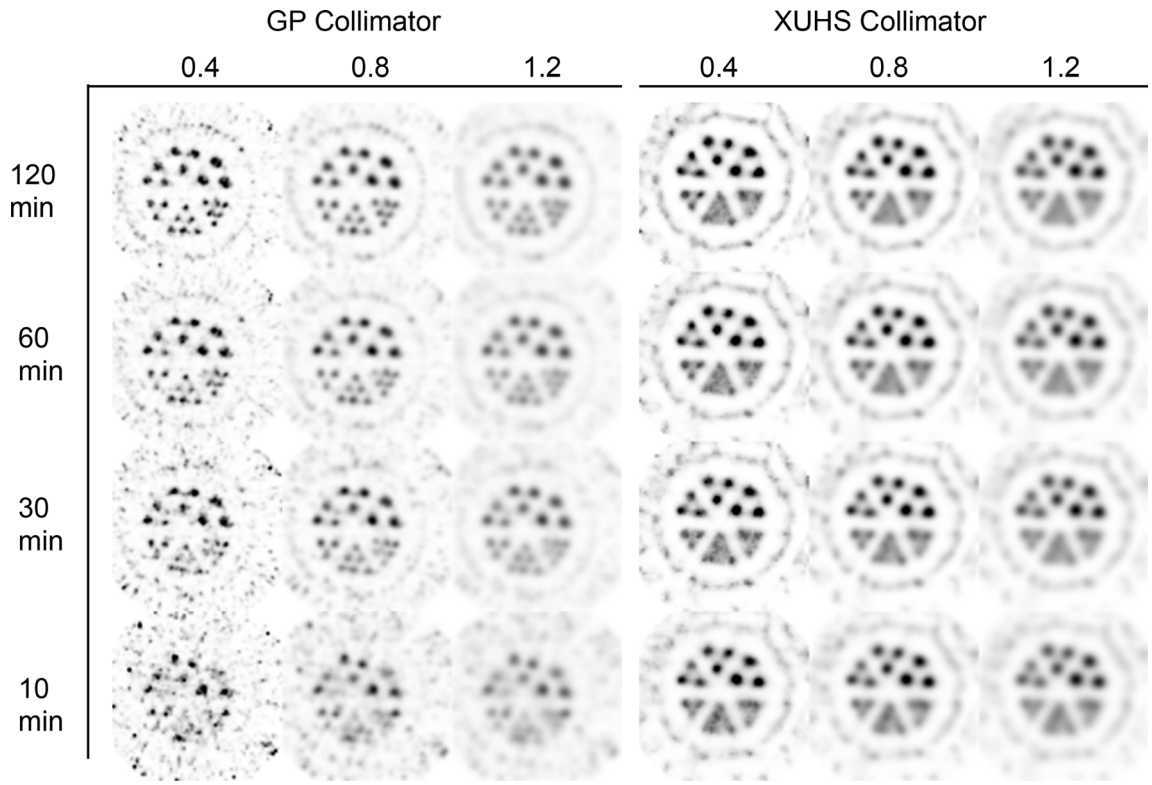

Fig. 3 Images of the radioactivity-filled rod phantom filled with 1 MBq of ^{195m}Pt acquired on the U-SPECT^{+} with the GP and XUHS collimator, increasing acquisition times, and 0.4-1.2 mm Gaussian blur filtering. GP = general purpose, XUHS = extra ultra-high sensitivity

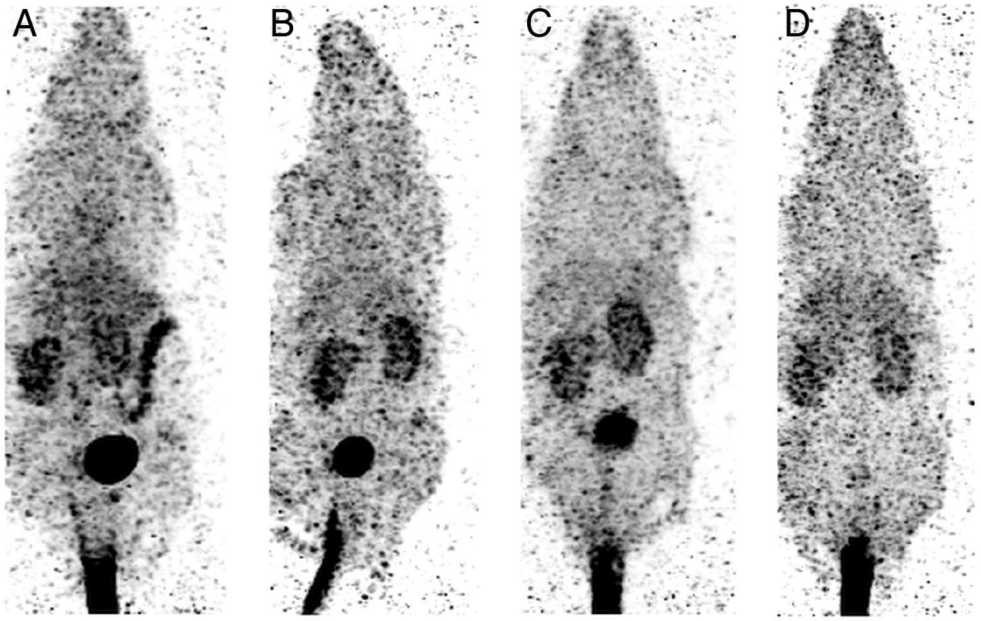

Fig. 4 Maximum intensity projection images of the four mice injected with 133 MB/kg ^{195m}Pt. All images were acquired on the NanoSPECT in 120 min. The mice were scanned either (**a**) immediately post injection, (**b**) 2 h post injection, (**c**) 4 h post injection, or (**d**) 24 h post injection

response over a wide activity range (0.035-4.36 MBq), suggesting that succeeding preclinical studies with radioactive cisplatin are possible.

For radiolabeling cisplatin, either ^{191}Pt, ^{193m}Pt, or ^{195m}Pt can be applied. The isotope ^{195m}Pt decays to ^{195}Pt with a half-life of 4.02 days, keeping the platinum compound and its biological behavior unaltered, and emitting 60-100 keV photons suitable for imaging. ^{191}Pt decays to ^{191}Ir and thus becomes a different molecule, which leads to regulatory challenges in human imaging studies because the chemical structure is no longer the same. ^{193m}Pt decays with a half-life of 4.33 days to the radioactive isotope ^{193}Pt, which has a relatively long half-life of 50 years. Moreover, the yield of suitable photons for imaging is much lower than for ^{195m}Pt [11]. Therefore, ^{195m}Pt is considered the isotope most suitable for medical imaging.

This feasibility study has several limitations. Firstly, a relatively low activity dose of ^{195m}Pt was administered to the mice. This was due to the relatively low specific activity of ^{195m}Pt and extravasation in the tail due to the highly acidic solution, but was compensated for by an scanning time up to a maximum of two h. However, the phantom images demonstrated that 30 min acquisition time is sufficient to obtain images of sufficient quality. Secondly, only four animals were scanned. Nevertheless, we found a good and statistically significant correlation among the three quantification methods SPECT, ex vivo gamma counting, and GF-AAS.

Thirdly, this study was performed with platinum-chloride and not cisplatin; with only 80% ^{195m}Pt present when injected in mice. The $H_2{}^{195m}PtCl_6$ solution was used for the preclinical imaging studies using the low energy gammas of ^{195m}Pt of 65 keV (22.4%), 67 keV (38.3%), and 99 keV (11.4%). The high energy gammas from the radionuclidic impurities ^{192}Ir (316 keV (82.8%), 296 keV (29.0%), 308 keV (29.7%) and 468 keV (47.8%)) and ^{199}Au (158 keV (40.0%) and 208 keV (8.7%)) were not supposed to interfere with the data acquisition. The same is reasoned for the high energy gamma of 191 keV (3.7%) of ^{197}Pt. The contribution of its 77 keV (17.0%) gamma will be minimal at the time of the data

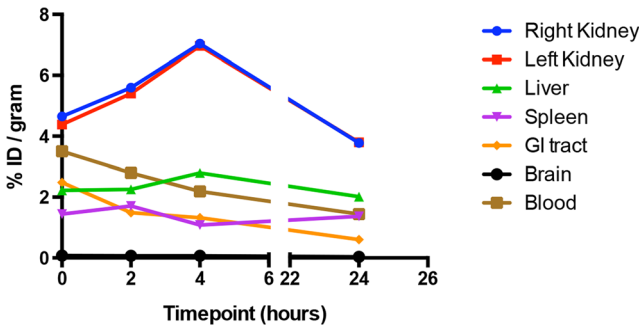

Fig. 5 The amount of ^{195m}Pt in different organs measured in a gamma counter expressed in %ID/gram over time. ID = injected dose

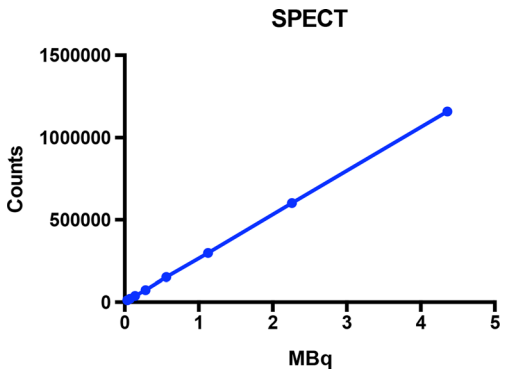

Fig. 6 Linearity of the NanoSPECT demonstrated with phantom measurements

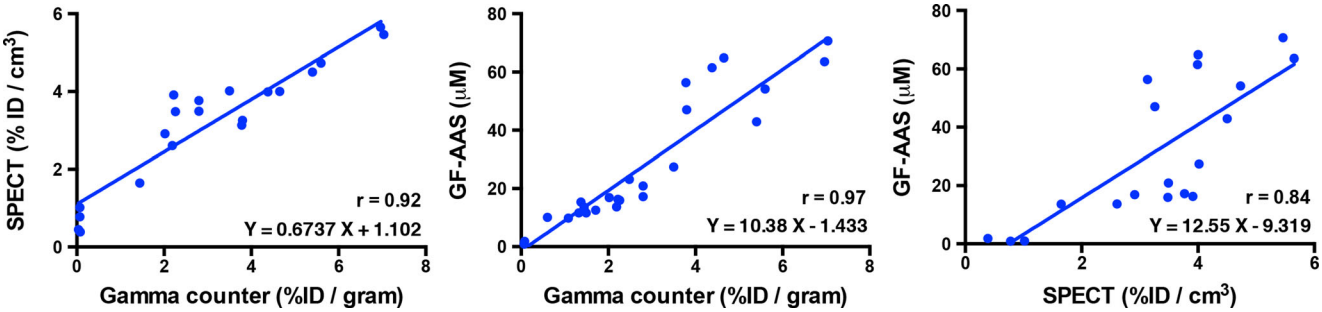

Fig. 7 Correlation between the three methods used to measure organ platinum uptake: SPECT, gamma counting, and GF-AAS. The Spearman correlation and a linear regression line are shown. GF-AAS = graphite furnace atomic absorption spectroscopy, ID = injected dose, SPECT = single photon emission computed tomography

acquisition, about 2 days after EOI, because of the relatively fast decay of ^{197}Pt, but could be reduced further by letting the solution decay for one more day. However, when platinum-chloride is used as a starting product for the synthesis of radioactive cisplatin, the iridium and gold impurities are removed, leading to a much higher radionuclide purity of ^{195m}Pt, which of course will be necessary when further (pre-)clinical studies are performed.

Fourthly, with the current specific activity, only 3-4 MBq of ^{195m}Pt could be injected in each mouse, leading to relatively high noise levels in the images. Experiments to increase specific activity are being performed at the moment, which are expected to improve image quality.

Despite these limitations, this study demonstrates that ^{195m}Pt SPECT is feasible in small animals and produces high-resolution quantifiable images. In the future, we plan to use ^{195m}Pt with higher specific activity for the labeling of cisplatin and other platinum containing drugs, and subsequently perform imaging studies in both small animal models and cancer patients. The ultimate aim will be personalized selection of those patients that are likely to benefit from cisplatin treatment or that might be susceptible to toxicities.

Conclusion

Preclinical ^{195m}Pt SPECT is feasible with acceptable tracer activities and acquisition times, and provides good image quality and accurate signal quantification. This makes biodistribution imaging of platinum compounds with ^{195m}Pt-SPECT a realistic possibility.

Compliance with ethical standards The authors declare no conflicts of interest. All applicable international, national, and/or institutional guidelines for the care and use of animals were followed. This article does not contain any studies with human participants performed by any of the authors.

References

1. Rosenberg B, Vancamp L, Krigas T. Inhibition of cell division in escherichia coli by electrolysis products from a platinum electrode. Nature. 1965;13:698–9.
2. O'Rourke N, Roqué i Figuls M, Farré Bernadó N, Macbeth F. Concurrent chemoradiotherapy in non-small cell lung cancer (Review). Cochrane Database Syst Rev. 2010;16, CD002140.
3. Green JA, Kirwan JJ, Tierney J, et al. Concomitant chemotherapy and radiation therapy for cancer of the uterine cervix. Cochrane Database Syst Rev. 2005;3, CD002225.
4. Lokich J, Anderson N. Carboplatin versus cisplatin in solid tumors: an analysis of the literature. Ann Oncol. 1998;9:13–21.
5. Browman G, Hodson D, Mackenzie R, Bestic N, Zuraw L. Choosing a concomitant chemotherapy and radiotherapy regimen for squamous cell head and neck cancer: a systematic review of the published literature with subgroup analysis. Head Neck. 2001;23:579–89.
6. Pignon JP, Bourhis J, Domenge C, Designé L. Chemotherapy added to locoregional treatment for head and neck squamous-cell carcinoma: three meta-analyses of updated individual data. Lancet. 2000;355:949–55.
7. Schaake-Koning C, van den Bogaert W, Dalesio O, et al. Effects of concomitant cisplatin and radiotherapy on inoperable non-small-cell lung cancer. N Engl J Med. 1992;326:524–30.
8. Bosch ME, Sánchez AJR, Rojas FS, Ojeda CB. Analytical methodologies for the determination of cisplatin. J Pharm Biomed Anal. 2008;47:451–9.
9. Lange RC, Spencer RP, Harder HC. Synthesis and distribution of a radiolabeled antitumor agent: cis-diamminedichloroplatinum (II). J Nucl Med. 1971;13:328–30.
10. Areberg J, Norrgren K, Mattsson È. Absorbed doses to patients from 191 Pt-, 193mPt- and 195mPt-cisplatin. Appl Radiat Isot. 1999;51:581–6.
11. Lange RC, Spencer RP, Harder HC. The antitumor agent cis-Pt(NH3)2Cl2: Distribution and dose calculations for 193mPt and 195mPt. J Nucl Med. 1972;14:191–5.
12. Lagasse L, Pretorius G, Petrilli E, Ford LC, Hoeschele J, Kean C. The metabolism of cis-dichlorociammineplatinum (II): distribution, clearance, and toxicity. Am J Obstet Gynecol. 1981;139:791–8.
13. Ewen C, Perera A, Hendry JH, McAuliffe CA, Sharma H, Fox BW. An autoradiographic study of the intrarenal localisation and retention of cisplatin, iproplatin and paraplatin. Cancer Chemother Pharmacol. 1988;22:241–5.
14. Los G, Mutsaers P, Lenglet W, Baldew G, McVie J. Platinum distribution in intraperitoneal tumors after intraperitoneal cisplatin treatment. Cancer Chemother Pharmacol. 1990;25:389–94.

15. Smith PS, Taylor DM. Distribution and retention of the antitumor agent 195mPt-cis-dichlorodiammine platinum (II) in man. J Nucl Med. 1974;15:349–51.
16. Iosilevsky G, Israel O, Frenkel A, et al. A practical SPECT technique for quantitation of drug delivery to human tumors and organ absorbed radiation dose. Semin Nucl Med. 1989;19:33–46.
17. Shani J, Bertram J, Russell C, et al. Noninvasive monitoring of drug biodistribution and metabolism: studies with intraarterial Pt-195m-Cisplatin in humans. Cancer Res. 1989;49:1877–81.
18. Areberg J, Bjorkman S, Einarsson L, et al. Gamma camera imaging of platinum in tumours and tissues of patients after administration of 191Pt-cisplatin. Acta Oncol. 1999;38:221–8.
19. Zamboni WC, Gervais AC, Egorin MJ, et al. Inter- and intratumoral disposition of platinum in solid tumors after administration of cisplatin. Clin Cancer Res. 2002;8:2992–9.
20. Sathekge M, Wagener J, Smith SV, et al. Biodistribution and dosimetry of 195mPt-cisplatin in normal volunteers. Nuklearmedizin. 2013;52:222–7.
21. Bailey DL, Willowson KP. An evidence-based review of quantitative SPECT imaging and potential clinical applications. J Nucl Med. 2013;54:83–9.
22. van der Have F, Vanstenhouw B, Ramakers RM, et al. U-SPECT-II: an ultra-high-resolution device for molecular small-animal imaging. J Nucl Med. 2009;50:599–605.